ASME Paper Tile: Impact of fluid substitution on the performance of an axial compressor blade cascade working with supercritical carbon dioxide

Authors: Carlos Tello, Alejandro Munoz, David Sanchez, Timoleon Kipouros, Mark Savill

ASME Journal Title: Journal of Engineering for Gas Turbines and Power

Volume/Issue __Volume 142, Issue 1_____ Date of Publication (VOR* Online) 11 December 2019____

ASME Digital Collection URL: https://asmedigitalcollection.asme.org/gasturbinespower/article/doi/10.1115/1.4045473/1068335/Impact-of-Fluid-Substitution-on-the-Performance-of

DOI: 10.1115/1.4045473

Journal of Nuclear Engineering and Radiation Science. Received September 30, 2019;
Accepted manuscript posted December 11, 2019. DOI:10.1115/1.4045473

Impact of Fluid Substitution on the Performance of an Axial Compressor Blade Cascade Working With Supercritical Carbon Dioxide

Carlos Tello[1]
Alejandro Muñoz[2]

[1]Department of Energy Engineering
University of Seville
41092 Seville, Spain
tello@us.es
ds@us.es

David Sánchez[1*]

[2]Total Direct Energie
3 Passage des entrepeneurs
75015 Paris, France
alejandro.munoz@celestpower.com

Timoleon Kipouros[3]
Mark Savill[3]
[3]School of Engineering
Cranfield University
Cranfield MK430AL, UK
t.kipouros@cranfield.ac.uk
mark.savill@cranfield.ac.uk

ABSTRACT

Recent research on turbomachinery design and analysis for supercritical Carbon Dioxide (sCO_2) power cycles has relied on Computational Fluid Dynamics. This has produced a large number of works whose approach is mostly case-specific, rather than of general application to sCO_2 turbomachinery design.

As opposed to such approach, this work explores the aerodynamic performance of compressor blade cascades operating on air and supercritical CO_2 with the main objective to evaluate the usual aerodynamic parameters of the cascade for variable boundary conditions and geometries, enabling 'full' or 'partial' similarity. The results present both the global performance of the cascades and certain features of the local flow (trailing edge and wake). The discussion also highlights the mechanical limitations of the analysis (forces exerted on the blades), which is the main restriction to applying similarity laws to extrapolate the experience gained through decades of work on air turbomachinery to the new working fluid.

This approach is a step towards the understanding and appropriate formulation of a multi-objective optimisation problem for the design of such turbomachinery components where sCO_2 is used as the operating fluid. With this objective, the paper aims to identify and analyse what would be expected if a common description of such computational design problems similar to those where air is the working fluid were used.

[*]Address all correspondence to this author. Email: ds@us.es

α	Flow angle
$\bar{c}_p$	Static pressure rise coefficient
β	Blade angle
γ	Isentropic exponent
μ	Dynamic viscosity
ϕ	Flow parameter
ϕ_{ext}	Extrapolated flow parameter
ρ	Density
σ	Solidity
θ	Camber angle
Ω	Aerofoil characteristics
ϖ	Total pressure loss coefficient
ξ	Stagger
a	Speed of sound
B_{th}	Blockage factor at the throat
c	Velocity
DF	Diffusion factor
e	Error of the extrapolated value
GCI	Grid Convergence Index
i_s	Stall incidence
l	Chord
p	Pressure
s	Pitch
T	Temperature
X	Axial force
Y	Tangential force
Z	Compressibility factor

INTRODUCTION

Status of Supercritical Carbon Dioxide Turbomachinery development. Literature review

Even if originally developed by Angelino in the late 1960s, the Supercritical Carbon Dioxide Power Cycle concept did not receive much attention for over three decades [1, 2]. It was not until the beginning of the past decade that it was brought back on the table as a potential substitute of Rankine cycles in High Temperature Nuclear Reactors [3].

Since then, there has been a substantial amount of work aimed at demonstrating the technical feasibility of the con-

cept [4, 5] and, also, at developing the tools and the understanding of the flow dynamics of weakly supercritical fluids in turbomachinery[1] [6–8]. Most of this research has focused on theoretical and experimental research based on very small radial compressors, as this is the most likely machine configuration of sCO_2 cycles under 50 MWe [9–11], whilst little attention has been paid to axial compressors [12–14].

The present work follows up on the previous research by the authors at University of Seville and Cranfield University, focused on characterising the fundamentals of supercritical carbon dioxide flows in diffusion devices. The very thorough research of supercritical CO_2 flows in conical diffusers presented in [15, 16] was extended to cascades of axial compressor blades in the understanding that this will be the configuration of choice, should the technology be applied in large nuclear reactors or coal power plants, as it has already been stated in literature [3, 17, 18]. Now, the work presented here aims to explore the differences that are to be expected when substituting supercritical CO_2 for the default working fluid in large throughput axial compresssors. This has already been done for radial machinery [6, 10, 15] but mostly on an individual, case-specific basis and not with the aim to draw general conclusions that could be applied to assess the general features of an axial machine. The next step will then be to use the general considerations drawn from this work to reduce the design-space where the blade geometry of the machine will be optimised for lowest losses and widest operating range.

Objectives

The objective of this work is to provide a fundamental discussion as to how the geometry and performance of a supercritical CO_2 compressor for power generation systems would be affected as compared to compressors in contemporary gas turbines (or power systems). This is more a fundamental approach than an attempt to yield a complete sCO_2 methodology, with the main objective to discuss the underlying dynamics of the flow.

EFFECT OF CHANGE IN WORKING FLUID

Forces on blades

Figure 1 shows a schematic representation of a compressor blade cascade of pitch/chord ratio *s/l*. The blades are aerofoils which, if placed in a fluid flow, bring about a change in flow velocity that is usually accompanied by a conversion of kinetic energy into pressure energy (or viceversa in the case of turbine vanes/blades). The application of mass and momentum conservation to the system in Figure 1 yields the forces that the fluid exerts on the blades when forced to change direction and velocity. This is shown in Figure 2 for the simple case of an incompressible, inviscid flow. The corresponding equations follow:

[1] 'Weakly' refers here to the fact that pressure and temperature remain above but close to their critical values.

$$\begin{cases} \rho \cdot s \cdot c_x^2 = p_1 \cdot s - p_2 \cdot s + X \\ \rho \cdot s \cdot c_x \cdot c_{y2} - \rho \cdot s \cdot c_x \cdot c_{y1} = -Y \end{cases} \tag{1}$$

$$\begin{cases} X = (p_2 - p_1) \cdot s \\ Y = \rho \cdot s \cdot c_x^2 \cdot (\tan \alpha_1 - \tan \alpha_2) \end{cases} \tag{2}$$

The utilisation of supercritical carbon dioxide in a standard compressor designed for atmospheric air is likely to cause a drastic increase of the forces on the blades (X and Y), determined by the ratio of inlet densities (1.1 kg/m^3 for air vs. 225 kg/m^3 for sCO_2). Such a rise of the corresponding stress is bound to be higher than the ultimate tensile strength of the material, thus triggering the catastrophic failure of the machine. In order to prevent this event, the following actions are possible:

- Reduce flow turning (deflection): this reduces the stage pressure ratio (aerodynamic load of the blade) which in turn increases the number of stages and the cost of the compressor.
- Reduce the inlet velocity of the flow: this increases the cross-sectional area of the stage (lower flow coefficient) and also reduces the average Reynolds number of the flow. Whilst the former effect means higher costs, the latter implies higher aerodynamic losses.
- Reduce pitch/chord ratio: increasing solidity ($\sigma = l/s$) reduces the aerodynamic load on each blade but increases friction losses. Trade-offs must be evaluated.

The aforedescribed situation confirms that axial compressors for supercritical carbon dioxide are bound to look different to standard compressors used in state-of-the-art gas turbines. Lower spans and higher solidities are foreseeable with the subsequent impact on compressor performance.

Blade Cascade Aerodynamic Performance

Similarity has been widely applied to the development of gas turbine engines, in particular for the extrapolation of the information gathered in low-speed testing of blade cascades (or even stages) to the particular set of operating conditions that would be encountered in the actual engine (including the working fluid) [19–21].

According to similarity rules, the aerodynamic performance of a blade cascade can be expressed through dimensional/non-dimensional groups in such a way that these remain unchanged despite changes in geometry or boundary conditions, as long as certain similarity parameters do not vary. This has been widely covered in literature and is taught in any undergraduate turbomachinery course. Nevertheless, when the working fluid is not an ideal gas or if the actual differences between the two 'similar' designs are very far from one another, applying similarity rules might lead to non-negligible errors. Moreover, it might even be the case that full similarity cannot be enforced/achieved [21].

The performance of an ideal gas flow across a compressor blade cascade comes determined by the outlet flow angle (α_2)

and total pressure loss (ϖ). These are dependent variables which rely on the following independent variables:

- Geometry:
  - Cascade: stagger (ξ), pitch (s) and chord (l).
  - Aerofoil (Ω): camber line (series), thickness distribution, inlet/outlet blade angles (β_1, β_2).
- Control variables: inlet flow angle (α_1) and velocity (c_1).
- Fluid variables (evaluated at the total inlet conditions): speed of sound (a_{01}), viscosity (μ), isentropic exponent (γ) and density (ρ_{01}).

$$\alpha_2, \varpi = f(\beta_1, \beta_2, s, l, \alpha_1, \alpha_2, \rho_{01}, \mu, \gamma, \Omega) \tag{3}$$

The application of the Pi Theorem of Buckingham to a particular aerofoil geometry (Ω) yields a somewhat simpler expression:

$$\alpha_2, \varpi = f(\theta, \xi, \sigma, \alpha_1, M_{01}, Re_{01}, \gamma) \tag{4}$$

Where θ is camber, $\sigma = l/s$ is solidity and M_{01} and Re_{01} are the Mach and Reynolds numbers at the inlet. It then follows that the performance of a blade cascade depends on a reduced number of geometric, aerodynamic/hydraulic and thermodynamic properties of the system. Recalling our previous statement, this means that if a higher solidity and/or lower camber were necessary in a supercritical compressor as a consequence of mandatory mechanical constraints, this would also have an effect on the aerodynamic performance of the machine. How and to what extent would efficiency and operating range change, and how this could be compensated for through optimisation of the aerofoil geometry is the prime driver of this research.

TEST CASE METHODOLOGY

General Features of the Adopted Modelling

The analysis presented in this work is organised in two steps. First, the global performance of a NACA 65-010 compressor cascade is studied in order to discuss the substitution of atmospheric carbon dioxide for air and, then, supercritical carbon dioxide for atmospheric CO_2. Then, local details of the flow field are evaluated for the same cases.

In as far as the turbulence model is concerned, the two-equation $k-\omega$ SST model is widely acknowledged to yield accurate results in turbomachinery design applications [22], also when supercritical carbon dioxide is used [7, 8][2]. It is

[2]Some examples of using k-ε models to simulate sCO_2 must nevertheless be acknowledged, for instance [7], even if the precaution of using proper near-wall treatment must be born in mind.

therefore used in this work in spite of the more stringent requirements concerning mesh refinement near the wall (in particular for the sCO_2 cases where Reynolds number is much higher). Air is treated as a perfect gas for faster computation whilst the properties of supercritical carbon dioxide are taken from the combination of Span & Wagner's equation of state (EOS) [23] and the thermal properties provided by CoolProp (thermal conductivity [24] and viscosity [25]); more information about the equation of state and the calculation of fluid properties can be found in [15, 26]. Finally, the model makes use of the COUPLED algorithm for the pressure-velocity coupling and a second order upwind interpolation scheme to ensure high accuracy of the results.

The authors would like to highlight that experimental validation of the work presented in this paper is, unfortunately, not possible today inasmuch as standard wind tunnels used for turbomachinery research do not enable cascade testing with CO_2 near the critical point (i.e., achieving with the compressibility factors of interest). The existing facilities worldwide (Sandia National Lab, Southwest Research Institute, Tokyo Institute of Technology, Czech Technical University in Prague, Technische Universitat Wien, Korea Advanced Institute of Science and Technology and others) can test the global performance of compressor and/or turbines at component and system levels but they do not enable blade cascade testing (including cascade performance parameters and local flow features). This would only be possible in a specific facility like the one designed by University of Seville in 2013 [27] which, unfortunately, was not constructed due to the lack of funding.

This problem of experimental validation was already experienced by the authors in a earlier work focused on the impact of fluid substitution (air to supercritical CO_2) on the performance of conical diffusers of different geometries [16]. In that work, based on the original experiments performed by Dolan & Runstadler for NASA in 1973 [28] (therefore with many commonalities with the present paper), Monje et al. presented the simulation platform and validated it for air against literature data. Then, given the lack of experimental data for sCO_2, a detailed discussion of the models and its different sources of uncertainty, including that brought about by grid resolution (based on the work by Celik [29]), was provided. The simulation platform used in the present work is the same as in Monje et al. [16] and the corresponding global performance calibration (for air) and assessment of grid resolution are presented in the next section.

Calibration and Mesh Independence Studies

The NACA 65 cascade is calibrated against the experimental results obtained by Lieblein some fifty years ago [30]. The reference case for calibration has the settings shown in Table 1 where the very similar values obtained from the experimental work and the model are noteworthy. The information shown refers to blade outlet angle α_2, diffusion factor DF and total pressure loss coefficient ϖ. These parameters and the static pressure rise coefficient $\bar{c}_p$ are described as follows:

$$\bar{c}_p = 2 \cdot \frac{p_2 - p_1}{\rho \cdot c_x^2} \tag{5}$$

$$\varpi = 2 \cdot \frac{p_{01} - p_{02}}{\rho \cdot c_x^2} \tag{6}$$

$$DF = (1 - \frac{c_2}{c_1}) + \frac{c_1 \cdot \sin\alpha_1 - c_2 \cdot \sin\alpha_2}{2 \cdot \sigma \cdot c_1} \tag{7}$$

The accuracy of the model is also checked for the mesh, shown in Figure 3. This is done through a Grid Convergence Index analysis with meshes having 20106, 34166 and 61900 cells. The analysis is based on the total pressure loss (ϖ) and static pressure rise ($\bar{c}_p$) coefficients and the results are shown in Table 2, not only for air but also for atmospheric and supercritical carbon dioxide (for a reference set of boundary conditions similar to those used later in the text). The very low *GCI* values obtained confirm that the results presented later in this paper are not affected by the mesh ($GCI_{ext}^{21} \ll 1$). In all cases throughout the analysis, near wall refinement is made where necessary to ensure that $y+ < 1$ and a convergence criteria of 10^{-6} is adopted for the residuals.

Similarity Conditions

The analysis is organised in two steps. In the first step, *full* similarity (both geometric and hydraulic)[3] is enforced for the working fluids considered. This is done with the aim to confirm that, under the similarity conditions set forth in the introduction, the performance of similar cascades is also similar despite the different *actual* conditions. A secondary objective is to confirm the extent to which the discussion in previous sections apply to supercritical fluids or if additional similarity parameters are needed.

As it happens, the condition of full similarity yields unrealistic cascade geometries (very small chords). Therefore, it is decided to release the similarity condition applied to Reynolds number (which is proportional to chord length) in order to enable longer chords. A new set of geometries is produced accordingly, wherein chord length remains the same as in the ideal CO_2 case, and their performance is again studied; this is termed *partial* similarity. Each case is set through a Matlab script iterating the following manipulating variables:

- Inlet Mach number. Mach number similarity is enforced through inlet velocity, which is itself controlled by outlet static pressure in the CFD code.
- Reynolds number: Reynolds number similarity is enforced through changes in blade chord. This implies an iterative meshing of the domain.
- Geometry: geometric similarity is enforced by using the same aerofoil series, camber and stagger angles and changing the pitch of the cascade (in order to keep solidity constant).
- Supercritical carbon dioxide: total temperature and pressure at the inlet are tuned in order to achieve the desired compressibility factor (Z).

[3]It is acknowledged that the term *full similarity* is actually incorrect inasmuch as γ cannot be tuned to the same value for each fluid. Nevertheless, the term is still used in the context of the paper.

OVERALL AERODYNAMIC RESULTS AND ANALYSIS

Global performance of the cascade

The overall performance of *fully* similar cascades is studied now. The region of low losses is arbitrarily defined as the range of incidence angles $[i_{(s+)},i_{(s-)}]$ for which the total pressure loss coefficient does not exceed twice the minimum value: $\varpi = 2 \cdot \varpi_{min}$.

The first case presented is a comparison between atmospheric air and carbon dioxide at atmospheric and supercritical pressures, all under *fully* similar conditions (air, CO_2 and $sCO_2(1)$). This is shown in Figure 4 where the total pressure loss and static pressure rise are plotted against incidence angle. The settings of each cascade are shown in Table 3:

- Geometry: stagger and solidity remain constant in all cases even if the absolute pitch and chord are different.
- Hydraulic similarity: Reynolds and Mach numbers remain constant.
- Properties of the working fluid: the isentropic exponent changes as this parameter cannot be controlled indirectly via another thermodynamic variable. The same happens to compressibility, which is different for supercritical CO_2.

Figure 4 comes to confirm that similarity is, indeed, a cross-cutting feature that can be applied between subcritical and supercritical flows. The performances of the three working fluids sharing the same similarity parameters are virtually indistinguishable; it is not until a close-up to the near stall conditions is observed (for a positive incidence beyond the region of low losses, $i > i_{s+}$) that minor differences due to the inherently different isentropic exponent (γ) become visible. It was already stated earlier that, of course, the cases are not fully similar but, at the same time, these observations reveal the much weaker effect of this latter similarity parameter (γ) on the performance of the cascade.

Moreover, the lower slope of the ϖ line in the region close to i_{s-} and i_{s+} in Figure 4 suggests a higher resistance against stall than for the other fluids and boundary conditions, what would eventually translate into a wider operating range of the machine. These conclusions apply to both energy conversion (kinetic energy into pressure energy, energy loss) and range (width of the region of minimum loss).

Further to the comparison in Figure 4, Table 3 reveals that the enforcement of full similarity when using air, CO_2 and sCO_2 brings about extremely short chords when the latter fluid is considered. This comes determined by the need to compensate for the two orders of magnitude higher density of supercritical CO_2, which cannot be fully offset by the lower speed of sound of the latter fluid. As a consequence of this, the resulting blade chord in the $sCO_2(1)$ case is just 1.2 mm, as opposed to approximately 130 and 90 mm for air and CO_2 at low pressure. This is why an additional case is plotted in Figure 4, $sCO_2(2)$, in which the chord is set to the same length as in the standard CO_2 case at low pressure (88.5 mm). This new restriction prevents full similarity and, in accordance, *Re* increases by two orders of magnitude (10^7). As shown in Figure 4, such a high *Re* reduces the irreversibility of the cascade, bringing about much lower losses and, therefore, higher static pressure rise.

The last two rows in Table 3 show the pressure rise and total pressure loss coefficients at the incidence for which the latter is lowest ($i_{ref} \approx -2.5$º). The first three similar cases have virtually the same values whilst the total pressure loss coefficient in the $sCO_2(2)$ case is more than halved, hence enabling a higher static pressure rise. The associated efficiency

rise in the actual machine would accordingly be significant (50% lower losses).

This pattern of pressure losses across elements of turbomachinery operating on air and supercritical carbon dioxide was already assessed by the authors in [16, 31] for the case of conical diffusers. Figure 5 shows the total pressure loss ($\varpi = K$) of one of these devices with given area ratio (D_{out}/D_{th}=4) and throat Mach number (M_{th}=0.2), operating with air and sCO_2 for different throat blockage factors[4] (B_{th}). It becomes evident that the total pressure loss is lower when supercritical carbon dioxide is used, irrespective of the blockage factor considered. The case labelled as L_{inlet}=50 mm, which stands for a diffuser with a 50 mm long inlet pipe, is fairly interesting because it accounts for the different boundary layer growth rate in each case. It is observed that sCO_2 yields about half the total pressure loss of air, which is in excellent agreement with the results shown in Figure 4.

It is to note that all the results shown in the paper so far are based on smooth aerofoils, as reported in Table 3, which is not the case in a real application. The effect of an increasing *Re* on the performance of a blade cascade with null roughness is a continuous reduction of total pressure losses. This is shown in Figure 6 where the total pressure loss coefficient of fully similar cascades operating on air and supercritical carbon dioxide is shown. Two cases are considered, null and positive roughness. In the former, the effect is as reported: decreasing ϖ for increasing *Re*. On the contrary, the effect of increasing *Re* when the aerofoils are not smooth vanishes when the critical value of *Re* is exceeded.

This is analysed further in Figures 7 and 8. The former shows the performance of fully similar cascades operating on CO_2, ideal and supercritical. Two cases are shown for each working fluid, smooth and rough, the latter of which assumes the same 10% relative roughness (absolute roughness over chord) of the blades regardless of the fluid. As expected, the smooth cascades exhibit better performance, with higher pressure rise and lower losses than the rough case. But what is more interesting is the fact that the performance is also the same when rough blades are considered, meaning that relative roughness is a similarity condition that can be used to compensate for changes in the surface finish of the aerofoils. This is in agreement with the observation by Wisler in [19], where he reports that the non-dimensional roughness ("scaled surface roughness") should also be accounted for as an additional similarity parameter .

Nevertheless, the results in Figure 7 are, to some extent, misleading given that it is unlikely that blades having chords differing by two orders of magnitude have the same relative roughness (see earlier discussion about the practicality of enforcing *Re* similarity for air and supercritical CO_2). This is explored in Figure 8 where the two sCO_2 cases are compared for the same absolute roughness (5μm); this is a more realistic comparison inasmuch as absolute roughness depends on the manufacturing process, which can be assumed to be the same in both cases. In this analysis, the better performance of $sCO_2(2)$ thanks to the higher *Re* is confirmed for either case: smooth or rough. Moreover, it is very relevant to see that the gap between $sCO_2(1)$ and $sCO_2(2)$ becomes larger when blades with the same absolute roughness are considered. This means that, in an actual turbomachinery with non-smooth walls, the performance enhancement brought about by using supercritical CO_2 is magnified.

[4]Blockage factor is the ratio from the free flow area to the geometric cross sectional are at the throat.

Local flow features

The foregoing results provide some hints as to how the new working fluid will expectedly impact the performance of the cascade. A step further is taken now by looking into the local flow features that might explain the trends observed. This is first assessed through the local static pressure distribution over the blade surface, shown in Figure 9. The situation is similar to Figure 4, with the fully similar cases merging into a single line and a visibly different line for the $sCO_2(2)$ case. Nevertheless, this pattern is not uniform since a closer look reveals that the non-dimensional loading is very similar on the suction side of the blade, for which differences between the $sCO_2(2)$ case and the three similar cases are hardly visible except for the last 5% of the chordwise coordinate. The close-up look in Figure 9 shows that a higher static pressure must be expected in the sCO_2 case as the trailing edge is approached.

The pressure side, on the other hand, experiences a just slightly higher non-dimensional pressure in the $sCO_2(2)$ case for chordwise coordinates lower than 0.5. Downstream of this point, the differences grow as the non-dimensional pressure of the latter case becomes higher than that of the other three cases: air, CO_2 and $sCO_2(1)$. Therefore, the conclusion drawn from Figure 9 is that the higher $\bar{c}_{p,sCO_2(2)}$ reported in Table 3 is explained by the blade having (non-dimensionally) a higher after-load. The root-cause of this localised difference is explored now.

Figure 10 shows the total pressure loss across the wake. The suction side is on the right hand side of the plot and the pressure side is on the left, as deduced from the higher contribution of the former to the total pressure loss. There are two interesting features that confirm the results presented earlier, in addition to the merging of the similar cases. First, it is evident that ϖ_{max} is approximately 50% lower for sCO2(2), as reported in Table 3. Then, also for this case, the wake is visibly narrower. Actually, this is the underpinning reason for the higher static pressure near the trailing edge in Figure 9. The smaller growth of the boundary layer in this region enables that kinetic energy be further converted in static pressure, as opposed to the other cases with lower *Re* where the flow is highly irreversible and hence a larger fraction of dynamic head is just lost. This applies to $\bar{c_p}$ not only on the pressure side but also on suction side in Figure 9. Indeed, the close-up shown in this plot reveals that the diffusion process in the $sCO_2(2)$ case proceeds further in the last 5% of the chordwise coordinate whereas it has already ceased in the other cases.

The flow pattern discussed in this section has a further read in terms of the velocity field. Indeed, Figure 11 shows the lower deviation of the outlet flow (from the blade angle) in the $sCO_2(2)$ case. The fact that the flow remains attached to the suction side of the blade helps reduce the pressure gradient between the pressure and suction sides near the trailing edge what, in turns, causes a lower flow turn in the wake. This reflects on a lower average outflow angle of the wake (i.e., higher deviation angle) and on a larger difference between the minimum and maximum local outflow angle in Figure 11.

Compressibility Effects at Higher Mach Numbers

The effect of running a compressor blade cascade at higher inlet Mach numbers is twofold: higher pressure loss coefficient (ϖ) and narrower operating range (smaller variation between i_{s-} and i_{s+}) [32]. This is verified when a supercritical fluid is used, as illustrated in Figure 12 where the performance of the reference cascade operating at 0.6 inlet Mach has been overlaid on the plot in Figure 4. Two observations are worth noting:

• The dashed lines corresponding to the higher operating Mach number yield an average ϖ_{min} that is some 50% higher than for the low Mach number case.

• The operating range in the high speed case is some 5° narrower than in the low speed case. This is because the high speed flow is more prone to stalling at high incidence angles, a behaviour that is also visible through the higher slope of the dashed ϖ curve towards the right end.

Figure 13 shows the non-linear effect of inlet Mach number on cascade performance and on the performance gap between the fully similar cases and the partly similar $sCO_2(2)$ case[5]. It is observed that, at higher Mach numbers, the static pressure rise of the cases with lower *Re* grows almost linearly whilst this growth is more than proportional for $sCO_2(2)$; the contrary is truth for total pressure loss, which grows more than linearly for the fully similar cases. This information is complemented by Figure 14 where the relative pressure rise (relative $\bar{c}_p$ with respect to the value for M_{01}=*0*) of each case is shown against inlet Mach number. Also in this plot, a reference is given by overlaying the resulting compressible static pressure rise coefficient according to the Prandtl-Glauert rule; this solution is representative of a linearised potential flow cascade whereby the compressible $\bar{c}_p$ is extrapolated from the incompressible value through a correction factor based on Mach number.

These plots confirm that the statements made in the preceding sections regarding the applicability of similarity when considering different working fluids, either subcritical or supercritical, are valid at high Mach numbers. This is evidenced by the fact that lines for the fully similar cases merge also at high M_{01} in Figures 12 and 13. Additionally, the information in Figure 13 confirms the observations highlighted before regarding the relative value of the total pressure losses in the fully and partially similar cases. Indeed,it is observed that the case with higher *Re*, $sCO_2(2)$, lies equidistant from the fully similar cases and the reference, ideal case (Pradntl-Glauert), which means that the losses experienced by the first set of plots are halved.

A final noteworthy feature in Figure 14 is the different pattern of relative pressure rise coefficient between the fully similar cases and the $sCO_2(2)$ case. At low Mach number, there is hardly any difference between all these cases but, at high Mach number, compressibility effects are stronger at high *Re*. This is due to the steeper pressure loss rise of the cases with lower *Re* for increasing M_{01}, Figure 13.

The information in this section confirms that the approach to turbomachinery design based on similarity applied to known cascade performance has the potential to yield an approximate geometry from which the subsequent optimisation process can be launched.

EFFECT ON BLADE LOADING AND FURTHER CONSIDERATIONS

Effect on Blade Loading

Earlier sections of this paper have confirmed that it is possible to apply similarity rules to the design of supercritical CO_2 turbomachinery despite the fact that the latter fluid does not follow the ideal gas behaviour. Indeed, even if full similarity yields unrealistic blade chords, the approach is still valid and the impact of releasing the constant *Re* condition can therefore be easily anticipated based on common turbomachinery design fundamentals.

[5]Results are limited to $M_{01} < 0.7$ because this is the critical Mach number for the reference cascade geometry.

The next step of the analysis goes back to the first section of this work where the forces on the blades were discussed. With the aim to verify the impact that fluid substitution has on the aerodynamic loads on the blades, Figure 15 shows the forces on the reference, partly similar air and $sCO_2(2)$ NACA 65 cascades reported in Table 3. It becomes visible that the aerodynamic forces are two orders of magnitude higher when operating on sCO_2 than in the reference air cascade, yielding 'bi-dimensional' stresses (per unit blade span) that are well beyond the limits of the material. Therefore, even if the much lower aspect ratio[6] b/d_{mean} of the sCO_2 machine (due to the much higher density of the latter fluid) would expectedly compensate for a fraction of this (thanks to the lower centrifugal and bending stresses), it can also be concluded that the aerodynamic design of the sCO_2 machine could not rely on the same design guidelines as for fully similar air cascades.

A further, interesting observation that is worthy of note in Figure 15 is the parallelism with Figure 4. Indeed, the tangential force is related to the aerodynamic load of the cascade and, as such, to the static pressure rise $\bar{c}_p$. Figure 4 reported earlier that the utilisation of sCO_2 at high *Re* ($sCO_2(2)$) delays the onset of stall because the flow remains attached to the suction side of the blade near the trailing edge (higher $\bar{c}_p$ at high i_+). This capacity of $sCO_2(2)$ to still increase the static pressure rise at high incidence angle translates into a different performance of the tangential force in Figure 15: whilst Y_{Air} decreases on the right end, the slope of $Y_{sCO_2(2)}$ is always positive. A final confirmation of this pattern is presented in Figure 16 where the relative values of the forces in Figure 15 is shown: $F = F_{sCO_2(2)}/F_{Air}$, with $F = X, Y$. The increase in $Y_{sCO_2(2)}$ far from the reference incidence ($i_{ref} \approx -2.5$º) becomes very clear in the plot, as it is also clear that the tangential force increases more than proportionally with respect to the axial force.

Further Considerations

A different approach to the same question is based on flow turn across the cascade, as already discussed in Figure 9. Indeed, Eq.(2) showed that the tangential force is related to flow deflection ($\varepsilon = \alpha_1 - \alpha_2$) which, for given incidence angle and blade camber, is equivalent to outlet flow angle. This was discussed in Figure 11 and it was claimed that the higher *Re* of $sCO_2(2)$ enables a thinner wake than in the other cases with either air or carbon dioxide (whether CO_2 or $sCO_2(1)$).

Following up on this rationale, Figures 17 and 18 show contours of total pressure and Mach number in *partly* similar NACA 65 compressor blade cascades operating on air and sCO_2. The plots confirm that the low velocity, low total pressure region is larger when air is used. This total pressure loss (ϖ) brings about a lower capacity to increase static pressure which explains the different behaviour near the trailing edge found in Figure 9. Moreover, not only is the wake thicker for air but it also has a different average flow angle in this case due to flow detachment from the suction side near the trailing edge; this causes that the streamlines do not follow parallel to the flow surface any longer and confirms the observations in Figure 11.

A final check is now made with respect to the impact of fluid substitution on the operating range of the machine. It was discussed earlier that the operating range of turbomachines working with sCO2 are expected to have a wider operating range, thanks to the arguably higher resistance to flow detachment at high incidence angles, Figure 4 and 5 [16]. This statement is now revisited, for which aim turbulent intensity is plotted for the same cascades as before, air and $sCO_2(2)$, but with a much higher incidence i =7.5º. From the information in the plots, it becomes clear that air detaches from the suction side of the

[6] b stands for blade height and d_{mean} for mean rotor diameter.

blade and gives way to a very large wake which tends to align with the direction of the chord, as opposed to the $sCO_2(2)$ flow which remains attached to the aerofoil. Under these boundary conditions, the air case can be considered stalled whilst the $sCO_2(2)$ case remains within the feasible operating range. Moreover, the plot also shows that the wake in the former case becomes aligned with the upper periodic boundary whilst these two lines are divergent (in the downstream direction) in the second case. This confirms the previous conclusions about the link between static pressure rise and deviation angle.

CONCLUSIONS AND FUTURE WORK

This work aims to provide the reader with some thoughts about whether or not the existing body of knowledge for preliminary turbomachinery design can be used to draft geometries for supercritical carbon dioxide compressors. The underpinning reason for this analysis is the widespread utilisation of optimisation tools for turbomachinery design and a general trend observed by the authors whereby researchers tend to rely on numerical calculations rather than on the lessons learned by experienced users. The fact that contemporary computers have almost unlimited computational capacity must not dismiss the vast experience accumulated by the industry in the last fifty years.

Upon these grounds, the paper provides five main conclusions:

- The application of similarity laws to the existing guidelines for the design of axial compressors is acceptable in spite of the markedly non-ideal gas behaviour of supercritical carbon dioxide. In other words, the similarity conditions (non-dimensional geometrical and hydraulic parameters) used in standard turbomachinery considering a quasi-ideal gas are still valid when supercritical fluids are involved.
- Nevertheless, full similarity cannot be achieved in a real case as it leads to impractical designs with very small sizes. This is of course due to the strong link between Reynolds number, density and chord.
- Accordingly, partial similarity (i.e. geometry and Mach number) proves to be the most sensible approach in order to obtain good preliminary designs of axial compressors for supercritical carbon dioxide. The adoption of partial similarity will also benefit from the positive effect of a much higher Reynolds number on the aerodynamic performance of the machine.
- For these same reasons, the operating range of a sCO_2 machine will expectedly be wider than in its air counterpart.
- All these conclusions are valid at higher Mach numbers for which compressibility effects become stronger. Moreover, the difference in performance between the partially similar supercritical Carbon Dioxide cases (with higher Reynolds number) with respect to the cases with air becomes larger at high speed.
- Unfortunately, the foregoing approach is limited by mechanical constraints owing to the much larger forces that act on the blades of the cascade when supercritical carbon dioxide is used.

Further to these conclusions, it is acknowledged that the mechanical impact of fluid substitution deserves a three-dimensional analysis in order to assess trade-offs between higher forces per unit span, lower aspect ratios (smaller flow path due to the much higher density of sCO_2) and higher solidity. Such analysis also enables a deeper analysis of secondary and tip leakage flows.

With all these in mind, it is thought that the conclusions of this paper provide the readers and the authors with the route for further research, with the ultimate objective to employ the same materials and manufacturing techniques as in contemporary air compressors. In addition, enhanced optimisation approaches like those previously applied for the successful design of axial compressors using air might need to be developed [33, 34].

REFERENCES

[1] Angelino, G., 1969. "Carbon dioxide condensation cycles for power production". *Journal of Power and Energy,* ***90***, pp. 287–295.

[2] Angelino, G., 1969. "Real gas effects in carbon dioxide cycles". In ASME Gas Turbine Conference and Product Show.

[3] Dostal, V., Driscoll, M., and Hejzlar, P., 2004. "A supercritical carbon dioxide cycle for next generation nuclear reactors". PhD thesis, Massachusetts Institute of Technology, Cambridge, MA.

[4] Wright, S., Radel, R., Vernon, M., Rochau, G., and Pickard, P., 2010. Operation and Analysis of a Supercritical CO_2 Brayton Cycle - SAND2010-0171. , Sandia National Lab, Albuquerque, NM.

[5] Utamura, M., Hasuike, H., Ogawa, K., Yamamoto, T. Fukushima, T., Watanabe, T., and Himeno, T., 2012. "Demonstration of Supercritical CO_2 Closed Regenerative Brayton Cycle in a Bench Scale Experiment (GT2012-68697)". In ASME Turbo Expo.

[6] Fuller, R., 2011. "Turbo-Machinery Considerations Using Super-Critical Carbon Dioxide Working Fluid for a Closed Brayton Cycle". In The 3^{rd} International sCO_2 Power Cycles Symposiumn.

[7] Rinaldi, E., Colonna, P., and Pecnik, R., 2012. "Computational Fluid Dynamics of a radial compressor operating with supercritical CO_2 (GT2012-69640)". In ASME Turbo Expo.

[8] Pecnik, R., Colonna, P., and Rinaldi, E., 2013. "Steadystate CFD investigation of a radial compressor operating with supercritical CO_2 (GT2013-94580)". In ASME Turbo Expo.

[9] Sienicki, J., Moisseytsev, A., Fuller, R., Wright, S., and Pickard, P., 2011. "Scale Dependencies of Supercritical Carbon Dioxide Brayton Ccycle Technologies and the Optimal Size for a Next-Step Supercritical CO_2 Cycle Demonstration". In The 3^{rd} International sCO_2 Power Cycles Symposiumn.

[10] Fuller, R., Preuss, J., and Noall, J., 2012. "Turbomachinery for Supercritical CO_2 Power Cycles (GT2012-68735)". In ASME Turbo Expo.

[11] Fleming, D., Holschuh, T., Conboy, T., Pasch, J., Wright, S., and Rochau, G., 2012. "Scaling Considerations for a Multi-Megawatt Class Supercritical CO_2 Brayton Cycle and Path Forward for Commercialization (GT2012-68484)". In ASME Turbo Expo.

[12] Wang, Y., Guenette, G., Hejzlar, P., and Driscoll, M., 2004. "Compressor Design for the Supercritical CO_2 Brayton Cycle (AIAA2004-5722)". In 2^{nd} International Energy Conversion Engineering Conference.

[13] Moisseytsev, A., and Sienicki, J., 2006. Development of a Plant Dynamics Computer Code for Analysis of a Supercritical Carbon Dioxide Brayton Cycle Energy Converter Coupled to a Natural Circulation Lead-Cooled Fast Reactor., Argonne National Lab, Argonne, IL.

[14] Takagi, K., Muto, Y., Ishizuka, T., Kikura, H., and Aritomi, M., 2010. "Research on Flow Charactreristics of Supercritical CO_2 Axial Compressor Blades by CFD Analysis". *Journal of Power and Energy,* ***4***, pp. 138–149.

[15] Monje, B., 2013. "Design of supercritical carbon dioxide centrifugal compressors". PhD thesis, School of Engineering, University of Seville.

[16] Monje, B., Sánchez, D., Chacartegui, R., Sánchez, T., Savill, M., and Pilidis, P., 2013. "Aerodynamic analysis of conical diffusers operating with air and supercritical carbon dioxide". *International Journal of Heat and Fluid Flow,* ***44***, pp. 542–553.

[17] Weiland, N., and Thimsen, D., 2016. "A Practical Look at Assumptions and Constraints for Steady State Modeling of sCO_2 Brayton Power Cycles". In The 5^{th} International sCO_2 Power Cycles Symposiumn.

[18] Miller, J., Buckmaster, D., Hart, K., Held, T., Thimsen, D., Maxson, A., Phillips, J., and Hume, S., 2017. "Comparison of Supercritical CO_2 Power Cycles to Steam Rankine Cycles in Coal-Fired Applications (GT2017-64933)". In ASME Turbo Expo.

[19] Wisler, D., 1984. "Loss Reduction in Axial-Flow Compressors Through Low-Speed Model Testing (84-GT-184)". In International Gas Turbine Conference and Exhibit.

[20] Zhu, N., Xu, L., and Chen, M., 1991. "Similarity Transformations for Compressor Blading (91-GT-123)". In International Gas Turbine and Aeroengine Congress and Exposition.

[21] Zou, Z., and Ding, C., 2018. "A new similarity method for turbomachinery with different working media". *Applied Thermal Engineering,* ***133***, pp. 170–178.

[22] Simoes, M. R., Montojos, N. R., and Moura, J. S., 2009. "Validation of turbulence models for simulation of axial flow compressors". In 20^{th} International Congress of Mechanical Engineering.

[23] Span, R., andWagner, W., 1996. "A New Equation of State for Carbon Dioxide Covering the Fluid Region from the TriplePoint Temperature to 1100 k at Pressures up to 800 MPa". *Journal of Physical and Chemical Reference Data,* ***25***, pp. 1509–1596.

[24] Scalabrin, G., Marchi, P., Finezzo, F., and Span, R., 2006. "A Reference Multiparameter Thermal Conductivity Equation for Carbon Dioxide with an Optimized Functional Form". *Journal of Physical and Chemical Reference Data,* ***35***, pp. 1549–1575.

[25] Fenghour, A., Wakeham, W., and Vesovic, V., 1998. "The Viscosity of Carbon Dioxide". *Journal of Physical and Chemical Reference Data,* ***27***, pp. 31–44.

[26] Hofer, D., and Moisseytsev, A., 2018. "Supercritical CO_2 Power Cycle Modeling and Fluid Properties Tutorial (GT2018-77461)". In ASME Turbo Expo.

[27] Sánchez, D., Monje, B., Chacartegui, R., Barrag'an, J. M., Pajuelo, E., G'omez, J. R., S'anchez, T., 2013. "Engineering a Pressurised Wind Tunnel Aimed at Developing CO_2 Turbomachinery (GT2013-94007)". In ASME Turbo Expo.

[28] Dolan, F., and Runstadler, P., 1973. "Pressure recovery performance of conical diffusers at high subsonic Mach numbers (nasa-cr-2299)". NASA, Washington.

[29] Celik, I., Ghia, U., Roache, P., and Freitas, C., 2008. "Procedure for estimation and reporting of discretization error in

CFD applications". *Journal of Fluids Engineering,* ***130***, pp. 1–4.

[30] Lieblein, S., 1965. "Experimental Flow in Two-Dimensional Cascades". In *Aerodynamic Design of Axial-Fow Compressors*, A. Johnsen and R. Bullock, eds. NASA, pp. 183–226.

[31] Monje, B., S'anchez, D., Chacartegui, R., S'anchez, T., Savill, M., and Pilidis, P., 2012. "Comparing the pressure rise of air and supercritical carbon dioxide in conical diffusers (GT2012-69835)". In ASME Turbo Expo.

[32] Dixon, S., 1998. *Fluid Mechanics, Thermodynamics of Turbomachinery*. Butterworth-Heinemann, Oxford.

[33] Kipouros, T., Jaeggi, D. M., Dawes, W. N., Parks, G. T., Savill, A. M., and Clarkson, P. J., 2008. "Bi-objective design optimization for axial compressors using Tabu Search". *AIAA Journal,* ***46***, pp. 701–711.

[34] Kipouros, T., Jaeggi, D. M., Dawes, W. N., Parks, G. T., Savill, A. M., and Clarkson, P. J., 2008. "Insight into high-quality aerodynamic design spaces through multi-objective optimization". *CMES: Computer Modeling in Engineering and Sciences,* ***37***, pp. 1–44.

θ	α_1	σ	DF_M	DF_L	$\alpha_{2,M}$	$\alpha_{2,L}$	$\varpi_{2,M}$	$\varpi_{2,L}$
[º]	[º]	[-]	[-]	[-]	[º]	[º]	[-]	[-]
30	45	1	0.407	0.427	24.7	23.9	0.01709	0.01704

Table 1. Calibration of the NACA 65 cascade operating on atmospheric air (subscripts M and L refer to values calculated by CFD model and by applying Lieblein's experimental correlation).

	AIR		CO_2		sCO_2	
	$\bar{c}_p$ [-]	ϖ [-]	$\bar{c}_p$ [-]	ϖ [-]	$\bar{c}_p$ [-]	ϖ [-]
ϕ_1	-6.300043	0.0179	-6.343194	0.0179	-6.614885	0.0230
ϕ_2	-6.267535	0.0175	-6.260755	0.0180	-6.599747	0.0233
ϕ_3	-6.329840	0.0179	-6.370872	0.0176	-6.617720	0.0238
ϕ_{ext}^{21}	-6.302112	0.0179	-6.346822	0.0180	-6.615551	0.0229
e_{ext}^{21}	0.5487%	0.0002%	1.3561%	0.1392%	0.2389%	1.7358%
GCI_{ext}^{21}	0.0411%	0.0001%	0.0715%	0.0227%	0.0126%	0.2821%

Table 2. Grid Convergence Index analysis for the NACA 65 cascade model.

Parameter	AIR	CO_2	sCO_2 (1)	sCO_2 (2)
Re_{01} [-]	$2.45 \cdot 10^5$	$2.45 \cdot 10^5$	$2.45 \cdot 10^5$	$1.76 \cdot 10^7$
M_{01} [01]	0.083	0.083	0.083	0.083
p_1 [bar]	1.012	1.017	75.236	75.237
T_1 [K]	299.6	299.7	314.6	314.6
ρ_1 [kg/m^3]	1.177	1.796	225.6	225.6
γ_1 [-]	1.402	1.293	3.236	3.236
μ_1 [-]	$1.79 \cdot 10^{-5}$	$1.37 \cdot 10^{-5}$	$2.03 \cdot 10^{-5}$	$2.03 \cdot 10^{-5}$
Z_1 [-]	1	1	0.56	0.56
c_1 [m/s]	28.8	22.4	17.9	17.9
Chord [m]	0.1297	0.0885	0.0012	0.0885
σ [-]	1	1	1	1
ξ [deg]	31.26	31.26	31.26	31.26
Roughness [-]	0	0	0	0
$\bar{c}_p(i = i_{\varpi_{min}})$ [-]	0.3006	0.3013	0.3000	0.3315
$\varpi(i = i_{\varpi_{min}})$ [-]	0.01701	0.0169	0.0173	0.0077

Table 3. Settings of the reference cascades. (1) stands for full similarity (i.e., equal Re) whereas (2) applies to constant chord and different Re.

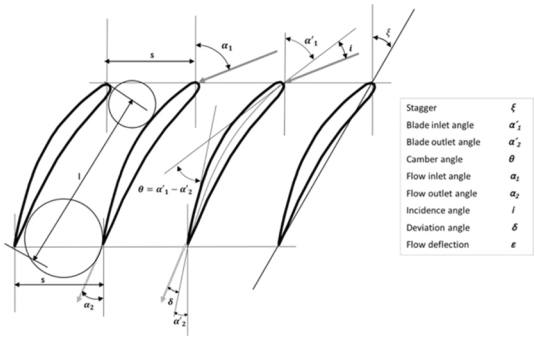

Fig. 1. Blade cascade definition and nomenclature.

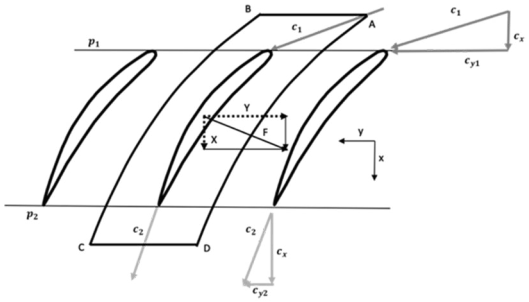

Fig. 2. Forces on a compressor blade cascade.

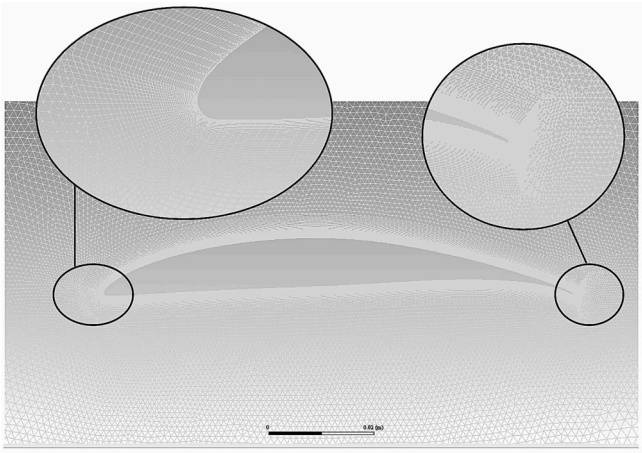

Fig. 3. Global view of the mesh and close-up of leading and trailing edges.

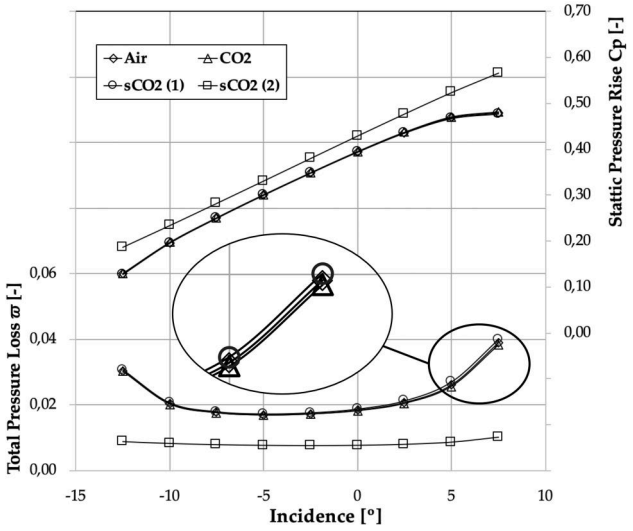

Fig. 4. Static pressure rise and total pressure loss for atmospheric air and atmospheric/supercritical CO_2 cascades.

Fig. 5. Total pressure loss of a conical diffuser of given area ratio ($AR = A_{out}/A_{in}$) and inlet Mach number [16].

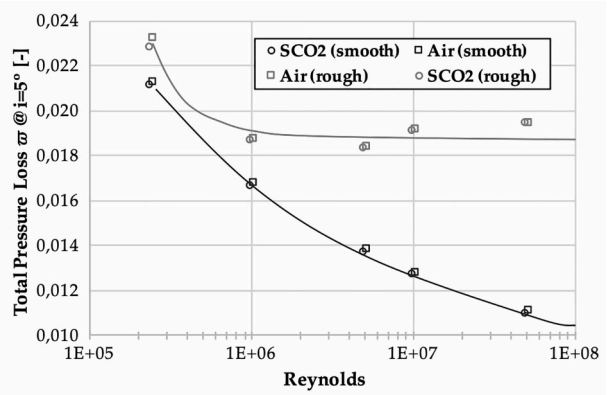

Fig. 6. Total pressure loss of air and supercritical CO_2 cascades using smooth and rough aerofoils.

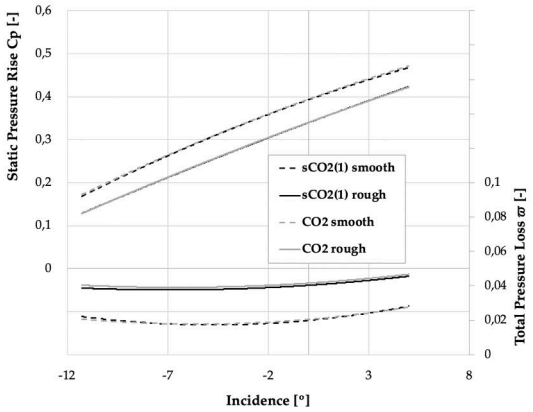

Fig. 7. Comparison between CO_2 and $sCO_2(1)$ cascades working with the same relative roughness (grain diameter over blade chord).

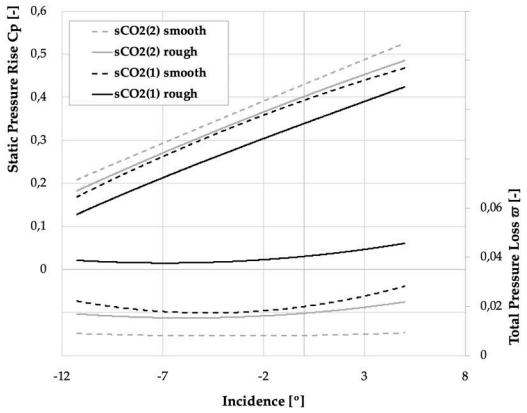

Fig. 8. Comparison between $sCO_2(1)$ and $sCO_2(2)$ cascades working with the same absolute roughness (5μm).

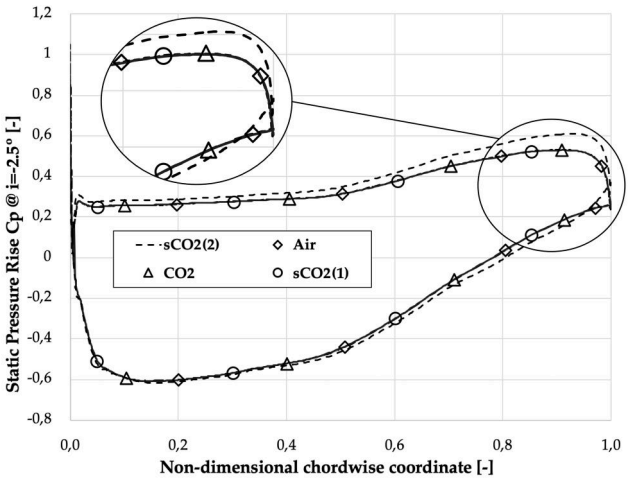

Fig. 9. Distribution of static pressure rise coefficient ($\bar{c}_p$) over the surface of the blade (non-dimensional aerodynamic loading). Incidence angle $i = -2.5$º.

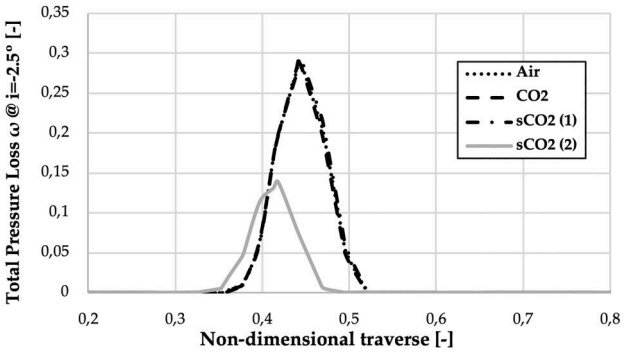

Fig. 10. Total pressure loss across the wake. Traverse located one chord downstream of the cascade. Incidence angle $i = -2.5$º.

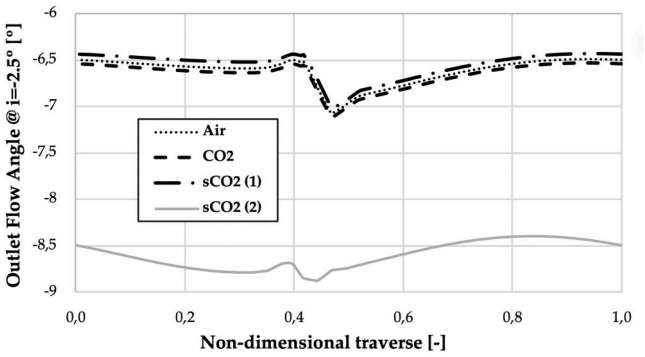

Fig. 11. Outlet flow angle (relative to chord line) across the wake. Traverse located one chord downstream of the cascade. Incidence angle $i = -2.5º$.

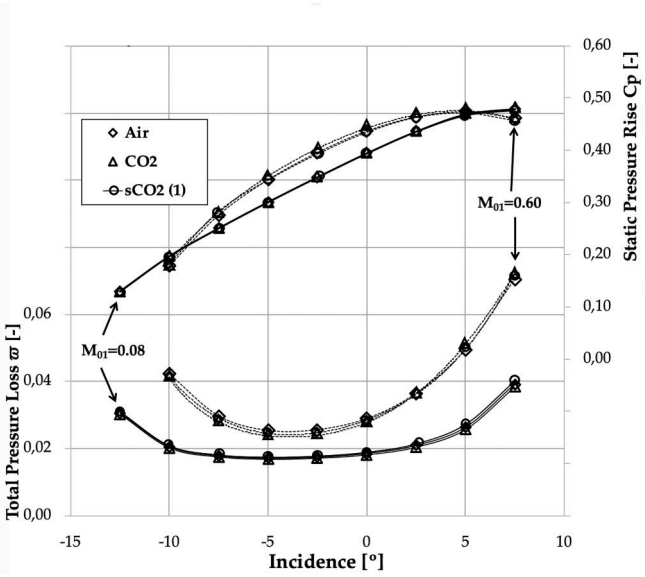

Fig. 12. Static pressure rise and total pressure loss for atmospheric air and atmospheric/supercritical CO_2 cascades. Dashed and solid lines correspond to M_{01}=0.6 and M_{01}=0.08 respectively.

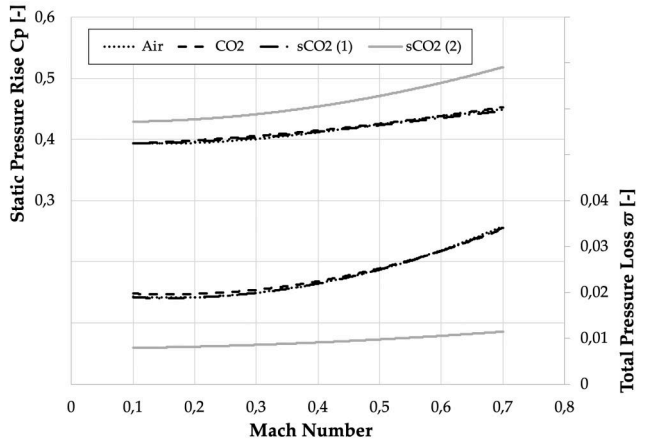

Fig. 13. Static pressure rise and total pressure loss for atmospheric air and atmospheric/supercritical CO_2 cascades.

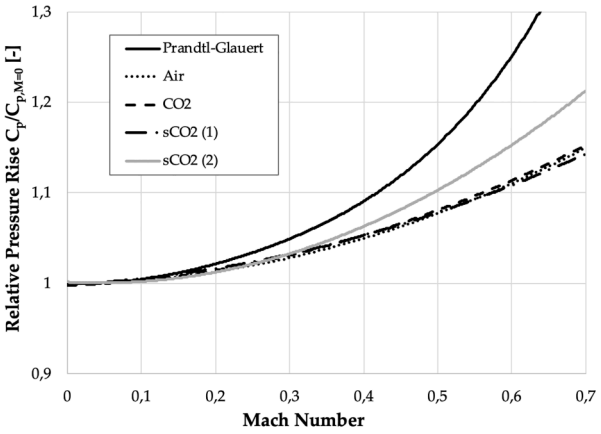

Fig. 14. Prandtl-Glauert transformation for the ideal case and for all the different cases studied.

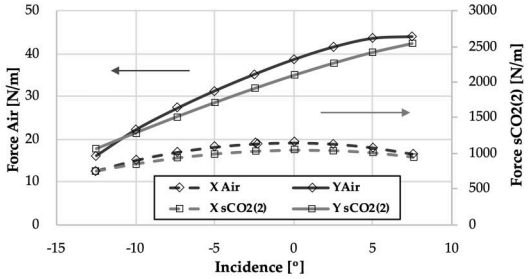

Fig. 15. Forces on blades across *partly* similar NACA 65 compressor blade cascades operating on air and supercritical carbon dioxide. Forces are reported per unit blade span.

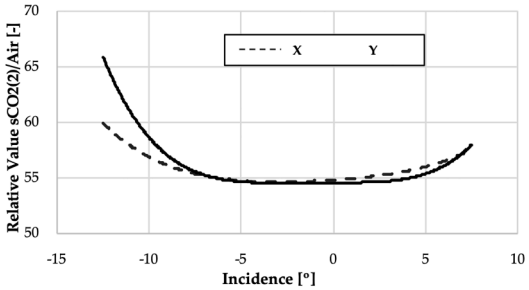

Fig. 16. Relative values of the axial and tangential forces (per unit span) on *partly* similar NACA 65 compressor blade cascades operating on air and supercritical carbon dioxide.

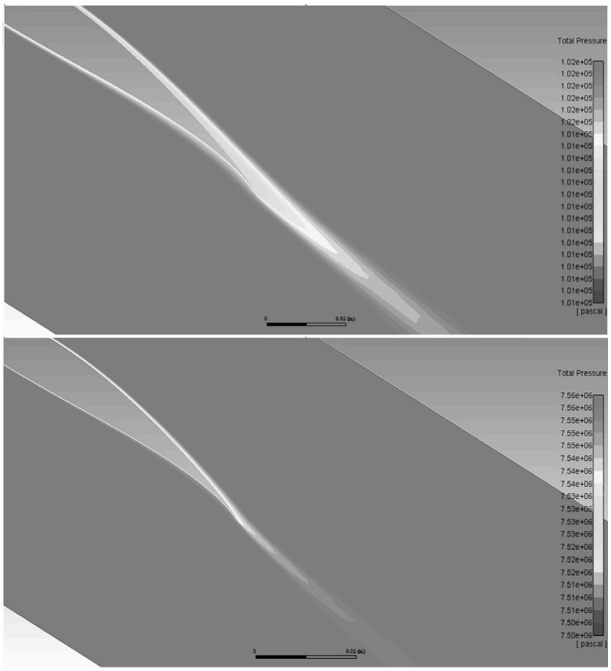

Fig. 17. Total pressure contours in *partly* similar NACA 65 compressor blade cascades operating on air (top) and supercritical carbon dioxide sCO_2(2) (bottom). Operating conditions reported in Table 3, with incidence i=-2.5º.

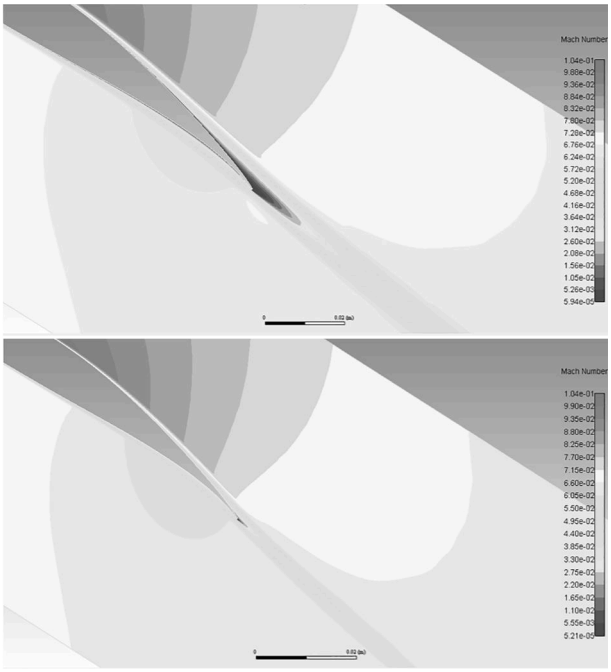

Fig. 18. Contours of Mach number in *partly* similar NACA 65 compressor blade cascades operating on air (top) and supercritical carbon dioxide sCO_2(2) (bottom). Operating conditions reported in Table 3, with incidence $i = -2.5$º.

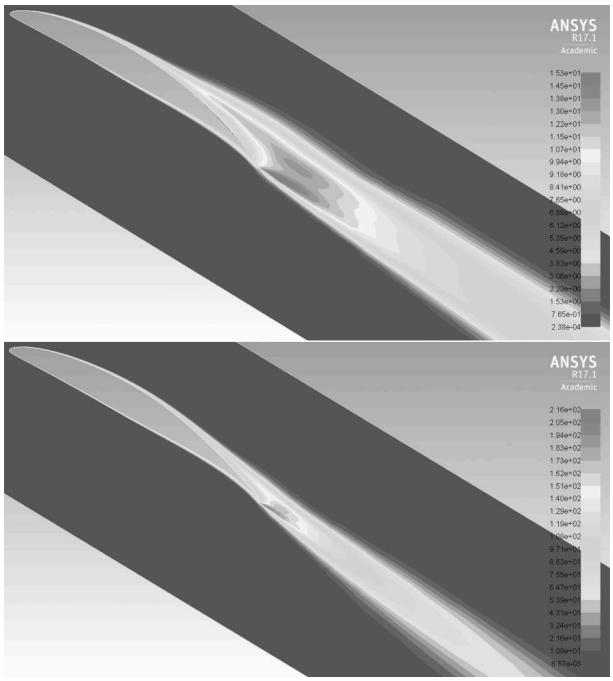

Fig. 19. Contours of turbulent intensity [%] in *partly* similar NACA 65 compressor blade cascades operating on air (top) and supercritical carbon dioxide sCO_2(2) (bottom). Operating conditions reported in Table 3, with incidence $i = 7.5$º.

Impact of fluid substitution on the performance of an axial compressor blade cascade working with supercritical carbon dioxide

Tello, Carlos

2019-12-11

Tello C, Sánchez D, Muñoz A, et al., (2020) Impact of fluid substitution on the performance of an axial compressor blade cascade working with supercritical carbon dioxide. Journal of Engineering for Gas Turbines and Power, Volume 142, Issue 1, January 2020, Article number 011019, Paper number GTP-19-1625

https://doi.org/10.1115/1.4045473